Research Square

Preprints are preliminary reports that have not undergone peer review.
They should not be considered conclusive, used to inform clinical practice,
or referenced by the media as validated information.

LSP1 in Spinal Cord Injury: Acute Inflammation-Related Biomarker and Potential Therapeutic Target

Feiyu Zhang
Affiliated Hospital of Nantong University
Yinuan Wang
Affiliated Hospital of Nantong University
Ruilin Chen
Taizhou Second People's Hospital
Jie Hao
Affiliated Hospital of Nantong University
Kai Zhao
Affiliated Hospital of Nantong University
YU Yao
yaoyu1122@sina.com
Affiliated Hospital of Nantong University

Research Article

Keywords: spinal cord injury, Mendelian randomization, neutrophils, LSP1, acute inflammation

Posted Date: April 25th, 2026

DOI: https://doi.org/10.21203/rs.3.rs-9347218/v1

License: This work is licensed under a Creative Commons Attribution 4.0 International License.
Read Full License

Additional Declarations: No competing interests reported.

Abstract

Spinal cord injury (SCI) is a severe traumatic disorder of the central nervous system, and acute inflammation represents a major obstacle to repair and functional recovery. This study aimed to identify reliable biomarkers and potential therapeutic targets for acute SCI using an integrated strategy of machine learning, Mendelian randomization (MR), and experimental validation. We analyzed two RNA-seq datasets (GSE226238 and GSE151371) to screen differentially expressed genes, and combined weighted gene co-expression network analysis (WGCNA), support vector machine (SVM), and Boruta algorithms to identify key biomarkers. LSP1 was identified as a critical candidate gene, which was positively correlated with neutrophil infiltration and showed a causal association with SCI risk by MR analysis. In vivo experiments using C57BL/6 mice revealed that LSP1 was significantly upregulated in acute SCI, and LSP1 knockout reduced neutrophil infiltration, decreased myeloperoxidase (MPO) expression, attenuated glial scar formation, and improved motor function recovery. Functional enrichment indicated that LSP1related genes were mainly enriched in the Apelin and Ctype lectin receptor signaling pathways. These findings demonstrate that LSP1 contributes to acute neuroinflammation by regulating neutrophil infiltration and may serve as a promising diagnostic biomarker and therapeutic target for acute SCI, providing new insights for precision antiinflammatory therapy.

Introduction

1.1 Research Background

Spinal cord injury (SCI) is a serious traumatic disease of the central nervous system that interrupts nerve signal transmission, leading to motor and sensory dysfunction. There are 250,000 to 500,000 new cases of SCI worldwide each year, which not only seriously reduces the quality of life of patients, but also brings a heavy economic burden[1]. SCI can be divided into acute phase (hours to days after injury) and chronic phase (weeks after injury): the acute phase is characterized by spinal cord tissue laceration and neuronal necrosis, while the chronic phase is associated with glial scar formation and neurodegenerative changes[2]. Currently, commonly used clinical treatments (such as surgical decompression, short-term neuroprotective therapy with methylprednisolone, etc.) are difficult to block the cascade of ischemia, inflammation and excitotoxicity[3]. Therefore, oxidative stress and inflammatory response in the acute phase are still the core challenges of SCI repair[4]. In recent years, emerging SCI treatment technologies (such as minimally invasive spinal cord stimulation, neural interfaces, and mesenchymal stem cell (MSC) therapy) have made some progress, but they have significant limitations: minimally invasive spinal cord stimulation is prone to decreased efficacy due to electrode displacement and infection; neural interfaces are expensive and carry the risk of intracranial infection [5]; and mesenchymal stem cell therapy faces problems such as uncontrollable cell differentiation and large individual differences [6]. More importantly, these treatment methods lack precise regulation of inflammatory molecular targets, making it difficult to

fundamentally reverse the pathological process. Therefore, it is urgent to screen highly reliable biomarkers and targeted therapy strategies [7].

Traditional studies using single-gene sequencing or single machine learning methods to explore differentially expressed genes (DEGs) related to SCI are often subject to confounding factors and reverse causal relationships. In contrast, Mendelian randomization (MR) uses single nucleotide polymorphisms (SNPs) as instrumental variables, which can effectively avoid reverse causal bias, reduce confounding effects, and ensure the validity of causal inference [8]; while machine learning can efficiently screen biomarkers related to the SCI microenvironment [9]. Therefore, this study combines the two methods and supplements them with experimental verification, which helps to deepen the understanding of the SCI inflammatory mechanism and thus provide potential therapeutic targets.

1.2 Research Content

This study used a “machine learning + Mendelian randomization” strategy to screen potential biomarkers related to acute inflammation in SCI[10]. First, gene expression datasets of SCI patients and healthy controls were obtained from the Gene Expression Omnibus (GEO). Differential expression analysis was used to screen DEGs, and weighted gene co-expression network analysis (WGCNA) was used to construct modules highly related to SCI. Candidate genes were obtained by taking the intersection of differentially expressed genes and module genes. Subsequently, machine learning algorithms were used to further screen and obtain 6 core genes. Based on the ROC curve analysis and box plot results in the validation set, LSP1 was finally identified as the key gene. This screening result is not accidental: previous studies have shown that LSP1 can regulate the rearrangement of the actin cytoskeleton in mouse macrophages, thereby affecting the migration of immune cells[11]. In addition, in diseases such as acute lung injury, LSP1 participates in neutrophil regulation and thus aggravates inflammatory damage, providing theoretical support for its role in SCI[12,13].

This study validated the findings through further Mendelian randomization analysis and ultimately completed in vivo validation using a mouse SCI model. In summary, this study preliminarily explored the possibility of LSP1 as a potential therapeutic target for SCI, and it is hoped that LSP1-targeted therapy may open up new avenues for combination therapy of SCI.

Materials and Methods

2.1 Data collection

This study obtained two datasets, GSE151371 and GSE226238, from the Gene Expression Public Database (GEO, https://www.ncbi.nlm.nih.gov/geo/), both of which were derived from SCI samples. After annotation and standardization of the datasets to eliminate batch effects, GSE226238 was finally set as the training set and GSE151371 as the validation set. Both datasets were obtained by RNA sequencing

(RNA-seq) technology. The gene SNP data used for MR analysis were all from the Genome-Wide Association Study Database (GWAS, https://gwas.mrcieu.ac.uk), with a sample size of 26,152 [14]. The Gene Ontology Database (GO) was constructed by the Gene Ontology Consortium and is a globally shared database containing three core categories: molecular function, cellular components, and biological processes. It is widely used in gene function annotation and differentially expressed gene analysis, providing support for related research. The Kyoto Encyclopedia of Genes and Genomes (KEGG) database covers systematics, genomics, and chemical information. With KEGG pathways as its core section, it presents metabolic pathways, signaling pathways, and other pathways in graphical form. Through gene localization, it can analyze the pathways involved by genes, explore the changing patterns of disease-related pathways, and deduce gene functions.

2.2 Data processing and differential gene screening

Based on a standardized preprocessing workflow built using the R language platform, this study employed the "Limma" package to perform differential expression analysis on SCI patient samples and control groups. DEGs were selected using the criteria of adjusted $p < 0.05$ and $log2FC > 1$ (where FC represents fold change). Heatmaps and volcano plots were generated using the pheatmap and ggplot2 packages for visualization.

2.3 WGCNA co-expression analysis

This study utilizes the WGCN system for systems biology research. The specific implementation steps are as follows: First, preprocessing of gene expression profile data is performed using the R language platform. Sample clustering analysis is used to accurately identify and remove abnormal samples and outliers, building a stable data foundation for subsequent analysis. Then, an adaptive soft thresholding method is used to construct a gene co-expression network that conforms to the requirements of a scale-free topology. Next, a dynamic tree pruning algorithm is used to cluster the expression characteristics of the entire genome to obtain co-expression modules with clear biological connotations. Genes within these modules typically exhibit significant synergistic regulatory patterns. To clarify the intrinsic relationship between co-expression modules and SCI clinical phenotypes, this study constructs a quantitative evaluation model based on the Pearson correlation coefficient. This model quantifies the degree of association between specific modules and SCI clinical phenotypes, thereby screening out core co-expression modules highly associated with the clinical characteristics of SCI samples. Finally, key module genes are further screened from these core modules. Then, the intersection of the DEGs selected in 2.2 with the genes in this module was used to obtain the intersection genes. GO and KEGG analyses were performed on these genes using the "clusterProfiler" R software package. The significance threshold was set to $p<0.05$, and the results were presented using visualization tools to explore potential mechanisms of action and biological processes.

2.4 Construction and validation of diagnostic models using multiple machine learning algorithms

This study adopted two machine learning algorithms: Support Vector Machine (SVM) and Boruta algorithm, and improved the reliability of the results by systematically screening overlapping genes [15]. SVM is a classic supervised learning algorithm. The core uses kernel function to process high-dimensional gene expression data. After optimizing the parameters by tenfold cross-validation, it finds the optimal hyperplane in high-dimensional space to distinguish SCI from normal samples, and then screens the potential biomarker genes that are key to classification according to feature weights. Boruta algorithm is based on random forest. It replicates the original genes and generates shadow features by shuffling. The two are trained together iteratively. Only when the importance of the original feature is consistently higher than that of the shadow feature is it determined to be a key gene related to SCI. Otherwise, it is removed. The intermediate features continue to iterate until the standard is met, and finally the core genes are screened. The overlapping genes of the two algorithms are visualized by Venn diagram to determine candidate biomarkers. The effectiveness was verified by two subsequent evaluations: one is to compare the expression differences of candidate genes in SCI and normal samples using box plots; the other is to evaluate its clinical diagnostic value for SCI by using ROC curves and AUC values.

2.5 Assessment of immune cell subtype composition and correlation analysis of immune cells

CIBERSORT, based on the linear support vector regression algorithm, estimates the relative proportions of 22 immune cell types in the sample (presented as a stacked bar chart) by integrating a reference matrix of known immune cell gene expression characteristics. The Wilcoxon test is used to analyze the differences in immune cell composition between the SCI sample and the control group. Spearman correlation analysis is used to explore the association between LSP1 gene expression and immune cell infiltration, and the results are visualized using lollipop plots generated by the ggplot2 package.

2.6 Mendelian randomization analysis

The data used in this study were obtained from the publicly available IEU Open GWAS database (https://gwas.mrcieu.ac.uk). The dataset ID for LSP1 used in this study is prot-a-576. The dataset ID for SCI-related data is finn-b-ST19_INJURY_NERVES_SPINAL_CORD_NECK_LEVEL. This dataset provides a list of 254 cases and 215,476 controls of European ancestry. To improve the reliability of Mendelian randomization results, this study rigorously screened the dataset: SNPs associated with the exposure factors and reaching genome-wide significance ($p<5\times10^{-8}$) were selected as instrumental variables (IVs). In the screening stage of genetic instrumental variables, a linkage disequilibrium screening threshold of $r^2 < 0.001$ was set, and the physical location interval of candidate SNPs was required to be > 10,000 base

pairs (kb) to eliminate linkage disequilibrium. This screening method successfully avoided the risk of false positive associations caused by co-segregation of genetic loci, ensuring that each included SNP can independently characterize the genetic features of the target gene, and providing genetic instrumental variables that conform to Mendelian randomization assumptions for subsequent causal inference.

After completing the effect allele correction of the exposure factors and outcome data, the inverse variance weighting (IVW) [16], weighted median (WMM) [17], MR-Egger method and weighted mode were used for analysis [18]. Among them, IVW is the most important method to assess causality. It integrates information of multiple instrumental variables with the inverse variance of the SNP effect estimate as the weight. The results are unbiased under the assumption of no level pleiotropy, providing a benchmark for exposure-outcome causal inference. At the same time, the heterogeneity was assessed by the Cochran's Q statistic. In the Cochran's Q test, the Q value $p<0.05$ indicates that there is heterogeneity among IVs [19]. The MR-Egger intercept test is used to assess level pleiotropy. The intercept term $p<0.05$ indicates that the effect exists. The results are visualized by scatter plot. The leave-one-out method can be used to screen SNPs that may have a potential impact on the IVW pooled estimate.

2.7 Methodological description of SCI experiments in C57BL/6 mice

Six-week-old C57BL/6 mice, weighing 20 g, were used as experimental animals in this study and were purchased from the Experimental Animal Center of Nantong University. All C57BL/6 mice were housed in a standardized humane environment with a constant 24-hour light-dark cycle. During the rearing period, all mice had free access to food and water. The LSP1 knockout (LSP1 KO) mice used in this study were constructed using CRISPR/Cas9 gene editing technology and were custom-produced by the Nanjing Model Animal Resource Center.

To accurately simulate the pathological state of common clinical spinal cord injury (SCI), this study established an animal model using the T10 segment spinal cord contusion method. Mice were anesthetized preoperatively by intraperitoneal injection of 1% sodium pentobarbital (dosage: 50 mg/kg), followed by shaving of the back hair and disinfection of the skin with iodine tincture. A small longitudinal incision was made along the long axis of the spine, and the skin and subcutaneous fascia were separated sequentially. After blunt dissection of the muscles, the T10 segment of the spinal cord was fully exposed. The Allen impact method was used to strike the surface of the T10 segment of the spinal cord. Successful establishment of the spinal cord contusion model was determined when the mouse exhibited limb twitching and complete relaxation of both hind limbs. One hundred C57BL/6 mice were randomly divided into three groups using a random number table: the sham-operated group underwent only laminectomy; the SCI group received only spinal cord contusion treatment; and the LSP1 gene knockout treatment group (LSP1 KO group) underwent spinal cord contusion treatment after LSP1 gene knockout. All mice were given antibiotics post-surgery to prevent infection and buprenorphine for

analgesia. Simultaneously, bladder manipulation was performed every 8 hours to assist urination until spontaneous urination function was restored. SCI tissue samples were collected on days 1, 3, and 7 of the experiment. As this was an exploratory study, the sample size was determined based on commonly used settings for behavioral and molecular marker detection in previous SCI animal studies.

To assess the recovery of motor function in mice after spinal cord injury (SCI), this study employed the following methods: 1. Gait analysis test for scoring. The entire experiment was blinded: neither the operators nor the recorders knew the mice's grouping information; each group of mice was operated independently by three randomly assigned researchers, and communication was avoided during the operation. The specific procedure for the gait analysis test was as follows: The mice were placed at the starting end of a walking platform and allowed to walk autonomously to the end; the entire walking process was recorded using a high-speed camera, and the system automatically extracted the footprint data; the footprint images were analyzed using Catwalk software to automatically identify and calculate core gait parameters such as step cycle, support distance, support time, swing time, braking time, and propulsion time. 2. BMS scoring: At predetermined time points, the mice were placed in an open area for free movement. Two uniformly trained observers, whose groupings were unknown, independently scored the mice based on hind limb joint activity, weight-bearing support, gait coordination, and trunk stability. If there were discrepancies between the two scores, the consistent results were reviewed and used for statistical analysis.

After euthanasia of mice, spinal cord samples were processed using two different methods for specific assays: (1)Polymerase chain reaction (PCR) assay: 3 mg of fresh tissue was rapidly placed into an enzyme-free grinding tube, an appropriate amount of pre-chilled Trizol lysis buffer was added, and the tube was immediately placed on ice to prevent RNA degradation. (2)Western blot (WB) assay: Another damaged segment of the spinal cord was rapidly isolated, rinsed with pre-chilled 0.9% saline to remove surface blood, blotted dry, and accurately weighed (approximately 5 mg). The sample was immediately placed into a grinding tube containing 1 mL of pre-chilled RIPA lysis buffer (with 1% protease/phosphatase inhibitor added before use).

All animal ethics-related procedures in this experiment were approved by the Animal Ethics Committee of Nantong University, with approval number S20230315-004.

2.8 Quantitative Real-Time Polymerase Chain Reaction(qRT-PCR)

Total RNA was extracted using Trizol reagent (Takara Bio, Japan). Complementary DNA (cDNA) was synthesized according to the instructions of the HiScript III RT SuperMix for qPCR (+ gDNA wiper) kit. Real-time quantitative PCR results were expressed as cycle thresholds (Ct values). The relative gene expression levels were calculated using the ΔΔCt method, with the formula: ΔΔCt = (Experimental group target gene Ct value - Experimental group internal reference gene Ct value) - (Control group target gene

Ct value - Control group internal reference gene Ct value). The forward primer for the LSP1 gene was 5’-CCACCTGGAGGAGTTGAGTCTGAG-3’, and the reverse primer was 5’-CCTGGGCTGCTGACATTTCTGG-3’. The forward primer for the β-actin gene was 5’-TGCGTGACATCAAGGAGAAG-3’, and the reverse primer was... 5’-TGCCAGGGTACATTGTGGTA-3’.

2.9 Immunofluorescence detection

Spinal cord tissue was collected for tissue microarray preparation: normal and damaged spinal cord samples were stored at -80°C and then thawed at -20°C for 30 minutes to equilibrate the temperature; 10 μm thick continuous sagittal sections were cut and attached to poly-L-lysine-coated slides.

The immunofluorescence staining procedure is as follows: First, the frozen sections were thawed at room temperature (RT) for 15 minutes, then fixed with 4% paraformaldehyde at room temperature for 15 minutes. The sections were then washed three times (5 minutes each) with phosphate-buffered saline (PBS) on a shaker. The sections were permeabilized with 0.1% Triton X-100 at room temperature for 10 minutes, and washed three times again with PBS. 5% bovine serum albumin (BSA) was added, and the sections were incubated at 37°C for 1 hour to block non-specific binding sites. The sections were then placed in a humidified chamber, and a primary antibody mixture diluted with 3% BSA (rabbit LSP1 antibody, 1:200 dilution; mouse Ly6G antibody, 1:150 dilution) was added. The sections were incubated overnight at 4°C, with isotype-matched IgG antibody used as a negative control.

The following day, the slides were warmed to room temperature for 30 minutes, washed three times with PBS, and then incubated with fluorescent secondary antibodies diluted with 3% BSA (Alexa Fluor 488-labeled goat anti-rabbit antibody, 1:500 dilution; Alexa Fluor 594-labeled goat anti-mouse antibody, 1:500 dilution) for 2 hours in the dark at room temperature. After washing three more times with PBS, 4',6-diamidinyl-2-phenylindole (DAPI, 1:1000 dilution) was added, and the slides were stained for 5 minutes in the dark at room temperature. The slides were then mounted with anti-fluorescence quenching mounting medium and stored at -20°C in the dark.

Fluorescence images were acquired using an Olympus FV3000 laser scanning confocal microscope with excitation wavelengths of 488nm (Alexa Fluor 488), 594nm (Alexa Fluor 594), and 405nm (DAPI). Five non-overlapping fields of view were selected in the lesion center and adjacent area and photographed at 10x and 40x magnification, respectively.

2.10 Western blot(WB)

Protein extraction procedure: Frozen spinal cord tissue stored at -80℃ was rapidly sheared into fragments on ice. The fragments were added at a ratio of 300 μL RIPA lysis buffer per 100 mg of tissue, and the samples were lysed using an ultrasonic cell disruptor under ice bath conditions. After incubating the lysis buffer on ice for 30 minutes, the samples were centrifuged at 4℃ and 12,000 rpm for 30

minutes. The supernatant was carefully transferred to a new enzyme-free centrifuge tube, which is the total protein extract. Protein concentration was determined according to the BCA protein quantification kit instructions, and then the protein samples were boiled at 100℃ for denaturation.

SDS-PAGE electrophoresis was performed using a 12% separating gel and a 5% stacking gel: 30 μg of protein was loaded onto each sample, and electrophoresis was first performed at 80 V until the sample entered the separating gel, then the voltage was adjusted to 120 V and electrophoresis was continued until completion. Before transfer, the PVDF membrane was activated by soaking it in methanol for 15 seconds; wet transfer was performed at 4℃ and 300 mA constant current for 90 minutes. After transfer, the membrane was placed on a shaker and washed three times (5 minutes each) with TBST buffer (1×Tris buffer solution containing 0.1% Tween-20), followed by blocking with 5% skim milk at room temperature for 1.5 hours.

The membrane was incubated overnight at 4℃ with LSP1 antibody and GAPDH antibody (primary antibody), which is an internal control gene. After washing and rewarming, the corresponding secondary antibody was added and incubated at room temperature for 1 hour. Then, the membrane was washed three times with TBST and once with TBS to remove residual Tween-20. For chemiluminescence detection, ECL reagent (equal volumes of solution A and solution B) was uniformly added to the membrane surface. Protein band images were acquired using a chemiluminescence imaging system, and the exposure time (5 seconds to 5 minutes) was adjusted according to the signal intensity.

2.11 Statistical Analysis

All statistical data were analyzed using GraphPad Prism 8.0 software (San Diego, USA). qPCR, Western blot, and immunofluorescence (IF) quantitative data are expressed as mean ± standard deviation ($\bar{x}\pm s$), and one-way ANOVA was used for inter-group comparisons. For behavioral data, CatWalk gait parameters and BMS scores were repeated measures data at multiple time points; repeated measures ANOVA was used to assess group, time, and their interactions; multiple post-hoc comparisons were performed when necessary. A p-value < 0.05 was considered statistically significant. qPCR, WB, and immunofluorescence quantification were analyzed using one-way ANOVA; BMS scores over time were analyzed using repeated measures ANOVA. *P < 0.05; **P < 0.01; ***P < 0.001; ****P < 0.0001.

2.12 Experimental reagents and instruments

Table 1 Experimental Materials

Reagents/Instruments	company
SPSS 26.0 software	IBM (USA)
R software (version 4.5.1)	R Foundation (USA)
Trizol reagent	Takara Bio (Japan)
HiScript III RT SuperMix for qPCR (+gDNA wiper) Kit	Nanjing Novizan Biotechnology Co., Ltd.
LSP1 gene-specific primers	Shanghai Sangon Biotech Co., Ltd.
β-actin gene internal reference primer	Shanghai Sangon Biotech Co., Ltd.
Real-time quantitative PCR reagent / SYBR Green	Nanjing Novizan Biotechnology Co., Ltd.
RNase Free H_2O	Tiangen Biotech (Beijing) Co., Ltd.
Real-time PCR instrument	Thermo Fisher Scientific, Inc.
PCR instrument	Thermo Fisher Scientific, Inc.
Anti-fluorescence quenching sealing tablets	Shanghai Beyotime Biotechnology Co., Ltd.
Rabbit anti-LSP1 antibody (1:200)	Abcam Corporation, USA
Mouse anti-Ly6G antibody (1:150)	Abcam Corporation, USA
Isotype-matched IgG antibodies	Abcam Corporation, USA
Alexa Fluor 488-tagged goat anti-rabbit antibody (1:500)	Invitrogen, USA
Alexa Fluor 594-tagged goat anti-mouse antibody (1:500)	Invitrogen, USA
4',6-Diamidinyl-2-phenylindole (DAPI)	Shanghai Beyotime Biotechnology Co., Ltd.
Olympus FV3000 Laser Scanning Confocal Microscope	Olympus Corporation of Japan
Poly-L-lysine coated slides	Jiangsu Shitai Experimental Equipment Co., Ltd.
RIPA pyrolysis fluid	Shanghai Beyotime Biotechnology Co., Ltd.
BCA Protein Quantitative Kit	Nanjing Novizan Biotechnology Co., Ltd.
SDS-PAGE electrophoresis reagents (acrylamide, methylenebisacrylamide, etc.)	Nanjing Chemical Reagent Co., Ltd.
methanol	Nanjing Chemical Reagent Co., Ltd.
Tris-buffered saline (TBS) chemiluminescence imaging system	Nanjing Chemical Reagent Co., Ltd. Thermo Fisher Scientific Inc. (USA)
TBST buffer (containing 0.1% Tween-20)	Nanjing Chemical Reagent Co., Ltd.

5% skim milk	Nanjing Weigang Dairy Co., Ltd.
LSP1 antibody	Abcam Corporation, USA
GAPDH antibody (internal control)	Abcam Corporation, USA
HRP-labeled secondary antibodies	Abcam Corporation, USA
ECL chemiluminescent reagents (solution A, solution B)	Shanghai Beyotime Biotechnology Co., Ltd.
PVDF membrane	Shanghai Beyotime Biotechnology Co., Ltd.
Ultrasonic cell disruptor	Ningbo Xinzhi Biotechnology Co., Ltd.
High-speed refrigerated centrifuge	Eppendorf, Germany
GraphPad Prism 8.0 software	GraphPad Software, Inc. (USA)
Biosafety cabinet	American Thermoelectric Company
Ice maker	Ningbo Aisbo Instrument Co., Ltd.
96-well plate	Corning Incorporated, USA
EP tubes	Corning Incorporated, USA
Phosphate-buffered saline (PBS)	Nanjing Chemical Reagent Co., Ltd.
0.1% Triton X-100	Nanjing Chemical Reagent Co., Ltd.
5% Bovine serum albumin (BSA)	Nanjing Chemical Reagent Co., Ltd.
Isotype-matched IgG antibody	Abcam Corporation, USA

Results

3.1 Batch effect correction and differentially expressed gene screening results

First, quality control, standardization, and batch effect correction were performed on 37 SCI samples and 9 control samples from the GSE226238 dataset (Figures 1A and 1B). Then, using log2FC > 1 and P < 0.05 as the screening threshold, a total of 929 differentially expressed genes were identified. Volcano plots and heatmaps were used to visualize the differentially expressed genes, with red representing upregulated genes and blue representing downregulated genes (Figures 1C and 1D).

3.2 WGCNA screens key SCI-related modules and candidate genes.

Cluster analysis was performed using the WGCNA package in R, and the cluster diagram was generated (Figure 2A). To meet the requirements of scale-free networks, a soft threshold of 5 was set, at which point the average connectivity approached 0 (Figure 2B), and the genes were clustered into 7 modules. The module-trait (SCI) association heatmap revealed that the blue module (MEblue) had the strongest correlation with SCI (r=0.59, p=2e-05), making it the most relevant key module for SCI (Figure 2C).

Further analysis of the blue module revealed a strong correlation between genes within it and SCI, with a correlation coefficient cor=0.79 (p=5.6e-103) (Figure 2D). Within this module, 477 genes most relevant to SCI were selected. These genes were then intersected with 929 differentially expressed genes selected from differential expression analysis, resulting in 61 genes, which served as a candidate set for subsequent functional analysis and core gene screening (Figure 2E).

3.3 Results of GO functional enrichment and KEGG pathway enrichment analysis of candidate hub genes

We performed enrichment analysis on these 61 candidate hub genes. KEGG pathway analysis showed that these candidate genes were significantly enriched in the Apelin signaling pathway, the C-type lectin receptor signaling pathway, the tuberculosis pathway, and the Kaposi's sarcoma-associated herpesvirus infection pathway. Among them, the Apelin signaling pathway is related to neural repair and inflammation regulation, while the C-type lectin receptor signaling pathway is involved in the immune response after SCI (Figure 3A). GO functional enrichment analysis showed that the candidate genes were enriched in functions such as ubiquitin-protein ligase binding, adenylate cyclase regulatory factor activity, and mitogen-activated protein kinase kinase binding. Specifically, ubiquitin-protein ligase binding is associated with neuroinflammation and axonal regeneration impairment after SCI; adenylate cyclase regulatory factor activity directly affects the efficiency of neural repair and the degree of inflammation after SCI by regulating cyclic adenosine monophosphate (cAMP) signaling; mitogen-activated protein kinase kinase binding is a core target in the pathological mechanism of SCI; and protein kinase activity regulation affects neural repair and functional recovery after SCI by regulating kinase activity (Figure 3B). These enriched pathways largely reflect that the inflammatory response after SCI is closely related to the prognosis of SCI.

3.4 Screening SCI core diagnostic genes based on machine learning algorithms

This study employed two machine learning algorithms: the Boruta algorithm and the Support Vector Machine Recursive Feature Elimination (SVM-RFE) algorithm. The Boruta algorithm used Z-score ranking to select 12 genes most relevant to SCI (Figure 4A), and the stability of each gene was verified by the number of classifier runs, ensuring the reliability and robustness of the results (Figure 4B). The SVM-RFE algorithm showed that when 38 feature genes were selected, the model achieved the highest accuracy (0.98) (Figure 4C) and the lowest error rate (0.02) (Figure 4D). By taking the intersection of the genes selected by the two algorithms, six core genes were finally obtained: EIF3B, ATP6V0C, IFRD1, LSP1, PYCR2, and FBRSL1 (Figure 4E).

3.5 Validation of expression characteristics and diagnostic value of core genes

In this study, box plots and ROC curves were plotted for the six selected genes in the training set. The results showed that the expression levels of EIF3B, FBRSL1, and PYCR2 in the SCI group were lower than those in the normal samples (Figure 5A). ROC curve analysis indicated that the AUC value of IFRD1 was only 0.502, suggesting extremely low diagnostic value (Figure 5B). Simultaneously, box plots and ROC curves were plotted for the above six genes using the GSE151371 dataset as the validation set (Figure

5C). The results showed that the p-values for ATP6V0C and PYCR2 were >0.05, indicating no statistically significant difference (Figure 5D).Therefore, this study first removed genes with abnormal expression trends from the training set, retaining ATP6V0C, IFRD1, and LSP1. Then, based on the box plot results from the validation set, genes with no statistical significance (i.e., ATP6V0C and PYCR2) were removed, leaving IFRD1 and LSP1. ROC curve analysis was performed on the six genes in both the training and validation sets. IFRD1 was removed based on its AUC value, and LSP1 was ultimately retained as a key pivot gene.

3.6 Immune cell infiltration characteristics and their correlation with LSP1 in the SCI model

To further explore the relationship between SCI and immune cells, this study used the CIBERSORT algorithm to predict immune cell infiltration. Figure 6A is a bar chart showing the proportion of 22 types of immune cells, which can visually demonstrate the differences in immune cell composition (Figure 6A). Compared with the control group, the proportion of 13 types of immune cells, including memory B cells, CD8+ T cells, γδ T cells, M1/M2 macrophages, and neutrophils, was significantly higher in the SCI group, suggesting that immune infiltration plays a key role in SCI (Figure 6B). To further verify the relationship between the key gene LSP1 and immune cells, this study conducted correlation analysis. The results showed that LSP1 was positively correlated with γδ T cells, activated memory CD4+ T cells, neutrophils, and M2 macrophages, and negatively correlated with resting NK cells and activated dendritic cells, suggesting that LSP1 may participate in the inflammatory process of SCI by regulating the above-mentioned immune cells (Figure 6C). The results in Figures 6B and 6C particularly show that neutrophils play an important role in the immune response after SCI and are closely related to LSP1. Therefore, it is speculated that LSP1 plays a significant role in SCI by influencing neutrophil-mediated immune responses, thereby regulating the immune response after SCI and ultimately affecting prognosis.

3.7 Mendelian randomization analysis reveals a potential causal link between LSP1 and the risk of SCI.

The MR method was used to explore the potential causal association between LSP and SCI. In the MR analysis, the causal effect value of single nucleotide polymorphisms (SNPs) combined with the genetic instrument variable in an IVW model under a random-effects model was used as the core statistical result. To ensure the reliability of the research conclusions, weighted median, simple pattern, and weighted pattern methods were further introduced for auxiliary validation, while the MR-Egger method was used to assess potential bias. Sensitivity analysis was performed by progressively eliminating individual SNPs to test whether the core result was excessively interfered with by specific genetic loci (Figure 7C). In the heterogeneity test, funnel plots were used to visualize the effect size distribution characteristics, and the MR-Egger intercept test was used to quantitatively identify level pleiotropy (Figure 7D). Finally, the impact of LSP1 on the risk of SCI was clarified; the stronger the SNP effect on LSP1, the higher the risk of SCI, supporting the causal relationship that increased LSP1 leads to increased SCI risk (Figures 7A, B). Further validation will be conducted using PCR, WB, and immunohistochemistry experiments.

3.8 PCR detection results of LSP1 gene knockout mouse SCI model

This experiment used two mouse genotypes: wild-type mice (LSP1+/+) and LSP1 knockout mice (LSP1-/-). Simultaneously, to dynamically observe changes in gene expression after injury, a sham control group (sham group) was set up for each genotype. Spinal cord tissue samples were collected from mice at three time points: 1 day, 3 days, and 7 days after SCI, and all samples were analyzed by real-time quantitative PCR.

Results from wild-type mice (LSP1+/+) showed that, compared with the sham-operated control group, the expression level of LSP1 gene was significantly increased 1 day after SCI, and then gradually decreased with the extension of time after injury. This expression pattern was completely consistent with the experimental expectations (Figure 8A).PCR results of LSP1 knockout mice (LSP1-/-) showed that no LSP1 gene expression signal was detected in samples at any time point (Figure 8A). Combined with the expression characteristics of wild-type mice, this result directly confirms the successful construction of LSP1 knockout mice in this experiment.

3.9 Western blot analysis of LSP1 and inflammatory cytokine MPO expression characteristics in SCI

To investigate the dynamic expression pattern of LSP1 after spinal cord injury (SCI) and its correlation with the expression of the inflammatory marker myeloperoxidase (MPO), and to evaluate the efficacy of therapeutic intervention, this study established SCI models using 6-week-old wild-type (LSP1+/+) and LSP1 knockout (LSP1−/−) mice, with sham-operated mice serving as controls for both genotypes. Spinal cord tissue was collected at 1, 3, and 7 days after SCI, and the protein expression levels of LSP1 and MPO were detected by Western blotting (WB). The results showed that in the SCI group, the protein levels of both LSP1 and the neutrophil infiltration marker MPO were significantly increased at 1 and 3 days post-injury, before declining at 7 days. In contrast, in the Sham group, the expression of LSP1 and MPO remained at baseline throughout the observation period, suggesting that their upregulation was a result of trauma-specific induction. Notably, the therapeutic intervention effectively inhibited the injury-induced increase in LSP1 and MPO, restoring their expression to levels comparable to those in the Sham group. These results suggest that this treatment strategy may exert a neuroprotective effect after SCI by inhibiting LSP1-mediated neutrophil infiltration and subsequent inflammatory response.

3.10 Immunofluorescence assay to verify the regulatory role of LSP1 in neural repair after SCI.

To investigate the regulatory role of LSP1 knockout in neural repair after spinal cord injury (SCI), this study established an SCI model using C57BL/6 mice and divided the animals into three groups: sham operation group (Sham group), spinal cord injury group (SCI group, $LSP1^{+/+}$), and LSP1 knockout intervention group ("Treat" group, $LSP1^{-/-}$). Immunofluorescence staining was used to detect the expression levels of axonal/neurofilament marker NF-200, neonatal neuron marker MAP2, mature neuron marker TUBB3, and glial scar marker GFAP in the lesion area.

The results showed that, compared with the Sham group, the fluorescence positive signals of NF-200 (Fig. 9A), MAP2 (Fig. 9B), and TUBB3 (Fig. 9C) were significantly downregulated in the SCI group, while the fluorescence positive signal of GFAP was significantly upregulated (Fig. 9D). These results suggest

that spinal cord injury can lead to axonal structural damage, neuronal loss, and excessive glial scarring. After LSP1 knockout intervention, compared with the SCI group, the positive expression of NF-200, MAP2, and TUBB3 was significantly restored in the treatment group (Fig. 9A–C), while the abnormally high expression of GFAP was significantly inhibited (Fig. 9D).

These results indicate that LSP1 knockout can be an effective intervention, associated with the recovery of axonal/neuronal related markers and the reduction of glial response, thus providing experimental evidence and potential targeted strategies for the neurorepair treatment of SCI.

3.11 Gait analysis was used to evaluate the effect of LSP1 knockout on the recovery of motor function in SCI mice.

To investigate the regulatory role of LSP1 in motor function recovery after spinal cord injury (SCI), 6-week-old mice were randomly divided into three groups: wild-type sham-operated group (Sham group), wild-type spinal cord injury group (SCI group), and LSP1 knockout spinal cord injury group ("Treat" group). Starting from 3 days post-surgery, the recovery of motor function in each group was dynamically assessed using a dual-indicator system combining gait analysis and Basso Mouse Scale (BMS) motor function scoring.

Behavioral results showed statistically significant differences in motor function among the three groups of mice. The Sham group showed no obvious gait abnormalities throughout the postoperative period, and its BMS score remained at a normal motor function level (9 points). In contrast, the SCI group exhibited typical gait disturbances due to spinal cord injury, characterized by significantly shortened stride length, imbalanced stance ratio, and significantly decreased limb coordination (Figure 10A). On postoperative day 3, the SCI group's BMS score was (0.73±0.08) points, confirming the successful establishment of the SCI model.

Notably, the core gait parameters (stride length, stance phase ratio, limb coordination, etc.) of the "Treat" group were significantly better than those of the SCI group (Figure 10A). Dynamic monitoring of BMS scores showed that the Treat group had significantly higher scores than the SCI group at all postoperative time points (Figure 10B), suggesting that LSP1 knockout can effectively improve motor dysfunction caused by SCI. Although there were still statistically significant differences in gait performance and BMS scores between the two injury groups (SCI and "Treat") and the Sham group, the gait characteristics and BMS scores of the "Treat" group showed a clear recovery trend towards normal motor function. By day 42 postoperatively, the motor function recovery of the "Treat" group was significantly better than that of the SCI group, and the difference was statistically significant.

Discussion

At present, SCI is a serious central nervous system injury, and its prognosis improvement still faces huge clinical challenges. The inflammatory response plays a core driving role in the pathological process after injury. After SCI occurs, the damaged spinal cord tissue quickly initiates an inflammatory cascade

response. This response not only directly recruits a large number of immune cells to infiltrate the injured site, but also triggers a series of secondary pathological damages such as ischemia and hypoxia, accumulation of excitatory amino acids, and oxidative stress, forming a vicious cycle of "inflammatory response - secondary damage", which directly destroys the microenvironment for nerve cell survival, hinders axonal regeneration and synaptic remodeling, and ultimately seriously affects the recovery of nerve function [20]. Although various intervention methods have been tried in clinical practice, the existing treatment strategies either focus on non-specific anti-inflammatory (such as glucocorticoids), which can only temporarily inhibit the inflammatory response but cannot block its continuous cascade amplification [21]; or rely on minimally invasive implantation devices (such as spinal cord electrical stimulation) or cell transplantation (such as mesenchymal stem cells), which not only make it difficult to accurately target the core inflammatory pathway, but also pose safety risks such as infection risk, device displacement, and immune rejection, and cannot achieve long-term and precise inflammatory regulation. Therefore, identifying key regulatory molecules of SCI-related inflammation and developing targeted therapies that are both specific and safe have become urgent needs for improving the prognosis of SCI patients and are also current research hotspots and challenges in the field of neurotrauma[22].

This study addresses this clinical challenge by innovatively employing an integrated research framework combining machine learning screening, MR causal validation, and in vitro/in vivo experimental validation, successfully overcoming the technical limitations of traditional research. In the target screening phase, we used machine learning algorithms to systematically analyze high-throughput sequencing data, initially screening candidate biomarkers associated with the acute inflammatory process of SCI from a large number of differentially expressed genes, significantly improving the efficiency and coverage of target screening. Subsequently, leveraging the unique advantages of Mendelian randomization analysis, we used genetic variation as an instrumental variable to effectively avoid confounding bias and reverse causality problems that are prone to occur in traditional observational studies. From an epidemiological perspective, we clarified the causal relationship between candidate biomarkers and acute inflammation in SCI, providing reliable causal evidence for subsequent experimental validation. Finally, through in vivo animal experiments, including SCI mouse models, we preliminarily validated that LSP1 is a core molecule regulating the acute inflammatory response after SCI. This research framework organically integrates bioinformatics, epidemiology, and experimental medicine techniques, not only efficiently and accurately identifying key anti-inflammatory targets but also providing a reference technical model for target discovery in SCI and other inflammation-related diseases, possessing significant methodological value.

At the mechanistic research level, this study has preliminarily revealed the core mechanism by which LSP1 participates in the acute inflammatory response after SCI: regulating the infiltration of neutrophils and the expression of the inflammatory factor MPO in the acute phase, directly affecting the intensity and duration of the inflammatory response after injury, and thus regulating the process of nerve repair and motor function recovery [23]. This discovery not only expands the functional understanding of LSP1 in inflammatory diseases, but also fills the gap in the study of the inflammatory initiation mechanism in

the acute phase of SCI, providing a new molecular perspective for elucidating the regulatory network of "immune cell infiltration-inflammatory response-neural function damage" [24, 25]. Moreover, compared with traditional pan-inflammatory targets (such as TNF-α, NF-κB), LSP1 has significant specific advantages [26]: it does not broadly inhibit the systemic inflammatory response, but precisely targets the key inflammatory link of "neutrophil aggregation" in the acute phase of SCI. Its excessive infiltration will aggravate tissue damage by releasing substances such as MPO, reactive oxygen species, and proteases, while the regulatory role of LSP1 is precisely focused on this pathological node, which is conceptually in line with the current development direction of precise anti-inflammatory intervention, but its clinical feasibility still needs further verification.

From a clinical translation perspective, the discovery of LSP1 provides an integrated approach to the diagnosis and treatment of SCI, showing promising application prospects. Firstly, LSP1 expression is significantly elevated during the acute phase of SCI, and ROC curve analysis demonstrates its good diagnostic value. LSP1 exhibits some diagnostic differentiation ability in existing data, but further validation with larger samples and clinical cohorts is needed. Secondly, animal experiments show that LSP1 knockout significantly inhibits neutrophil infiltration and MPO expression in the lesion area of SCI mice, reduces local inflammation, and promotes axonal regeneration and neurological function recovery, confirming its potential as a therapeutic target. Compared to existing treatments, LSP1-targeted interventions do not require implantation devices and can be regulated through various pathways such as small molecule drugs, antibodies, and gene editing. This approach is simpler to operate, safer, and can, to some extent, address the issues of insufficient precision and poor safety in traditional treatments, providing a new direction for precision anti-inflammatory treatment of SCI. In addition, GO/KEGG enrichment analysis showed that LSP1-related genes were mainly enriched in the Apelin signaling pathway, the C-type lectin receptor signaling pathway, and other pathways related to immune regulation and cell survival. This suggests that LSP1 may regulate neutrophil infiltration and neural repair through multiple pathways, providing a theoretical basis for subsequent multi-target combined anti-inflammatory strategies. This study still has several limitations. First, the publicly available transcriptome datasets used for bioinformatics screening have a relatively limited sample size, and the training and validation sets are insufficient to fully cover the clinical heterogeneity of SCI, potentially affecting the robustness and extrapolation of the model. Second, although this study combined machine learning, Mendelian randomization, and animal experiments for multi-level validation, the exposure and outcome data used in the Mendelian randomization analysis were all from publicly available databases, and their population background, phenotypic definitions, and data collection methods are not entirely consistent with the research objectives of this study; therefore, related causal inferences still require careful interpretation. Third, this study mainly validated the role of LSP1 in the acute inflammatory response of SCI at the overall knockout level, but it has not yet further elucidated its specific expression and precise molecular mechanisms in different cell types, especially lacking in-depth elucidation of LSP1's regulation of neutrophil recruitment, activation, and downstream signaling pathways. Finally, this study used animal models for validation and has not yet included clinical patient samples for prospective testing; therefore, the clinical translational value of LSP1 as a diagnostic biomarker and therapeutic target still needs

further evaluation. Future advancements can be made in the following areas: First, expand the inclusion of publicly available datasets and clinical samples, and conduct multi-center, tiered external validation to improve the stability and reliability of LSP1 as a biomarker for the acute phase of SCI. Second, combine single-cell transcriptome sequencing, spatial transcriptome, and immune colocalization technologies to clarify the spatiotemporal expression characteristics of LSP1 in neutrophils and other inflammation-related cells. Third, further analyze the downstream molecular network of LSP1-mediated neutrophil infiltration and inflammation amplification at the mechanistic level, and elucidate its intrinsic connection with oxidative stress, immune microenvironment remodeling, and neural repair. Fourth, explore intervention strategies based on small molecule inhibitors, antibodies, or targeted delivery systems, and validate their safety and efficacy in models that more closely resemble clinical scenarios. Fifth, conduct translational research using patient peripheral blood or cerebrospinal fluid samples to evaluate the application potential of LSP1 in early diagnosis, disease stratification, and efficacy monitoring.

Conclusion

1. This study, by integrating machine learning screening, MR causal validation, and in vitro and in vivo functional validation, preliminarily confirmed that LSP1 is a candidate causal biomarker and potential therapeutic target for regulating acute inflammation after SCI.

2. The results show that LSP1 can significantly affect the intensity of the inflammatory response after SCI by regulating neutrophil infiltration and the expression of the inflammatory cytokine MPO, thereby influencing the recovery process of motor function.

3. This finding provides new ideas and strategies for precision anti-inflammatory treatment of SCI.

References

1. Nuechterlein, A., et al., Strengths, gaps, and future directions on the landscape of ethics-related research for spinal cord injury. Spinal Cord, 2023. 61(9): p. 477-482.https://doi.org/10.1038/s41393-023-00897-z
2. Wagner, F.C., Jr., J.C. VanGilder, and G.J. Dohrmann, Pathological changes from acute to chronic in experimental spinal cord trauma. J Neurosurg, 1978. 48(1): p. 92-8.https://doi.org/10.3171/jns.1978.48.1.0092
3. Bracken, M.B., et al., Administration of methylprednisolone for 24 or 48 hours or tirilazad mesylate for 48 hours in the treatment of acute spinal cord injury. Results of the Third National Acute Spinal Cord Injury Randomized Controlled Trial. National Acute Spinal Cord Injury Study. Jama, 1997. 277(20): p. 1597-604.https://doi.org/10.1001/jama.1997.03540440031029
4. Shen, Y.J., Y.C. Huang, and Y.C. Cheng, Advancements in Antioxidant-Based Therapeutics for Spinal Cord Injury: A Critical Review of Strategies and Combination Approaches. Antioxidants (Basel), 2024. 14(1).https://doi.org/10.3390/antiox14010017

5. Jaszczuk, P., et al., Advances in Neuromodulation and Digital Brain-Spinal Cord Interfaces for Spinal Cord Injury. Int J Mol Sci, 2025. 26(13).https://doi.org/10.3390/ijms26136510
6. Lyu, Z., et al., Cause and consequence of heterogeneity in human mesenchymal stem cells: Challenges in clinical application. Pathol Res Pract, 2024. 260: p. 155354.https://doi.org/10.1016/j.prp.2024.155354
7. Zou, W., et al., Mesenchymal stem cell transplantation ameliorates inflammation in spinal cord injury by inhibiting lactylation-related genes. Cytokine, 2025. 191: p. 156960.https://doi.org/10.1016/j.cyto.2025.156960
8. Yin, S., et al., Trends in Mendelian randomization in neurological disease research: a bibliometric analysis. Front Neurol, 2025. 16: p. 1525481.https://doi.org/10.3389/fneur.2025.1525481
9. Yao, Y., et al., Identification of Ifitm1 as a Pivotal Gene in Mouse Spinal Cord Injury Using Comprehensive Machine Learning Algorithms. Mediators Inflamm, 2025. 2025: p. 6149780.https://doi.org/10.1155/mi/6149780
10. Yuan, X., et al., Key Targets in Subacute Spinal Cord Injury Identified by Bioinformatics and Mendelian Randomization. World Neurosurg, 2025. 198: p. 123966.https://doi.org/10.1016/j.wneu.2025.123966
11. Cervero, P., et al., Lymphocyte-specific protein 1 regulates mechanosensory oscillation of podosomes and actin isoform-based actomyosin symmetry breaking. Nat Commun, 2018. 9(1): p. 515.https://doi.org/10.1038/s41467-018-02904-x
12. Liu, L., et al., LSP1 is an endothelial gatekeeper of leukocyte transendothelial migration. J Exp Med, 2005. 201(3): p.409-18. https://doi.org/10.1084/jem.20040830
13. Le, N.P., et al., Leukocyte-specific protein 1 regulates neutrophil recruitment in acute lung inflammation. Am J Physiol Lung Cell Mol Physiol, 2015. 309(9): p. L995-1008.https://doi.org/10.1152/ajplung.00068.2014
14. Hayes, B., Overview of Statistical Methods for Genome-Wide Association Studies (GWAS). Methods Mol Biol, 2013. 1019: p. 149-69.https://doi.org/10.1007/978-1-62703-447-0_6
15. Alhamzawi, R. and H.T.M. Ali, The Bayesian adaptive lasso regression. Math Biosci, 2018. 303: p. 75-82.https://doi.org/10.1016/j.mbs.2018.06.004
16. Mounier, N. and Z. Kutalik, Bias correction for inverse variance weighting Mendelian randomization. Genet Epidemiol, 2023. 47(4): p. 314-331.https://doi.org/10.1002/gepi.22522
17. Bowden, J., et al., Consistent Estimation in Mendelian Randomization with Some Invalid Instruments Using a Weighted Median Estimator. Genet Epidemiol, 2016. 40(4): p. 304-14.https://doi.org/10.1002/gepi.21965
18. Bowden, J., G. Davey Smith, and S. Burgess, Mendelian randomization with invalid instruments: effect estimation and bias detection through Egger regression. Int J Epidemiol, 2015. 44(2): p. 512-25.https://doi.org/10.1093/ije/dyv080
19. Xiao, G., et al., Causality of genetically determined metabolites on anxiety disorders: a two-sample Mendelian randomization study. J Transl Med, 2022. 20(1): p. 475.https://doi.org/10.1186/s12967-

022-03691-2
20. Zhang, Y., et al., Acute spinal cord injury: Pathophysiology and pharmacological intervention (Review). Mol Med Rep, 2021. 23(6).https://doi.org/10.3892/mmr.2021.12056
21. Singh, P.L., et al., Current therapeutic strategies for inflammation following traumatic spinal cord injury. Neural Regen Res, 2012. 7(23): p. 1812-21.https://doi.org/10.3969/j.issn.1673-5374.2012.23.006
22. Zhu, S., et al., Biomaterial-based strategies: a new era in spinal cord injury treatment. Neural Regen Res, 2025. 20(12): p. 3476-3500.https://doi.org/10.4103/NRR.NRR-D-24-00844
23. Kubota, K., et al., Myeloperoxidase exacerbates secondary injury by generating highly reactive oxygen species and mediating neutrophil recruitment in experimental spinal cord injury. Spine (Phila Pa 1976), 2012. 37(16): p. 1363-9.https://doi.org/10.1097/BRS.0b013e31824b9e77
24. Zhu, P., et al., [Leukocyte-specific protein 1 (LSP1): A key regulator of cytoskeletal dynamics and leukocyte function]. Xi Bao Yu Fen Zi Mian Yi Xue Za Zhi, 2025. 41(8): p. https://doi.org/750-755.10.13423/j.cnki.cjcmi.009995
25. Wang, C., et al., Modulation of Mac-1 (CD11b/CD18)-mediated adhesion by the leukocyte-specific protein 1 is key to its role in neutrophil polarization and chemotaxis. J Immunol, 2002. 169(1): p. 415-23.https://doi.org/10.4049/jimmunol.169.1.415
26. Le, N.P., et al., Leukocyte-specific protein 1 regulates neutrophil recruitment in acute lung inflammation. Am J Physiol Lung Cell Mol Physiol, 2015. 309(9): p. L995-1008.https://doi.org/10.1152/ajplung.00068.2014

Figures

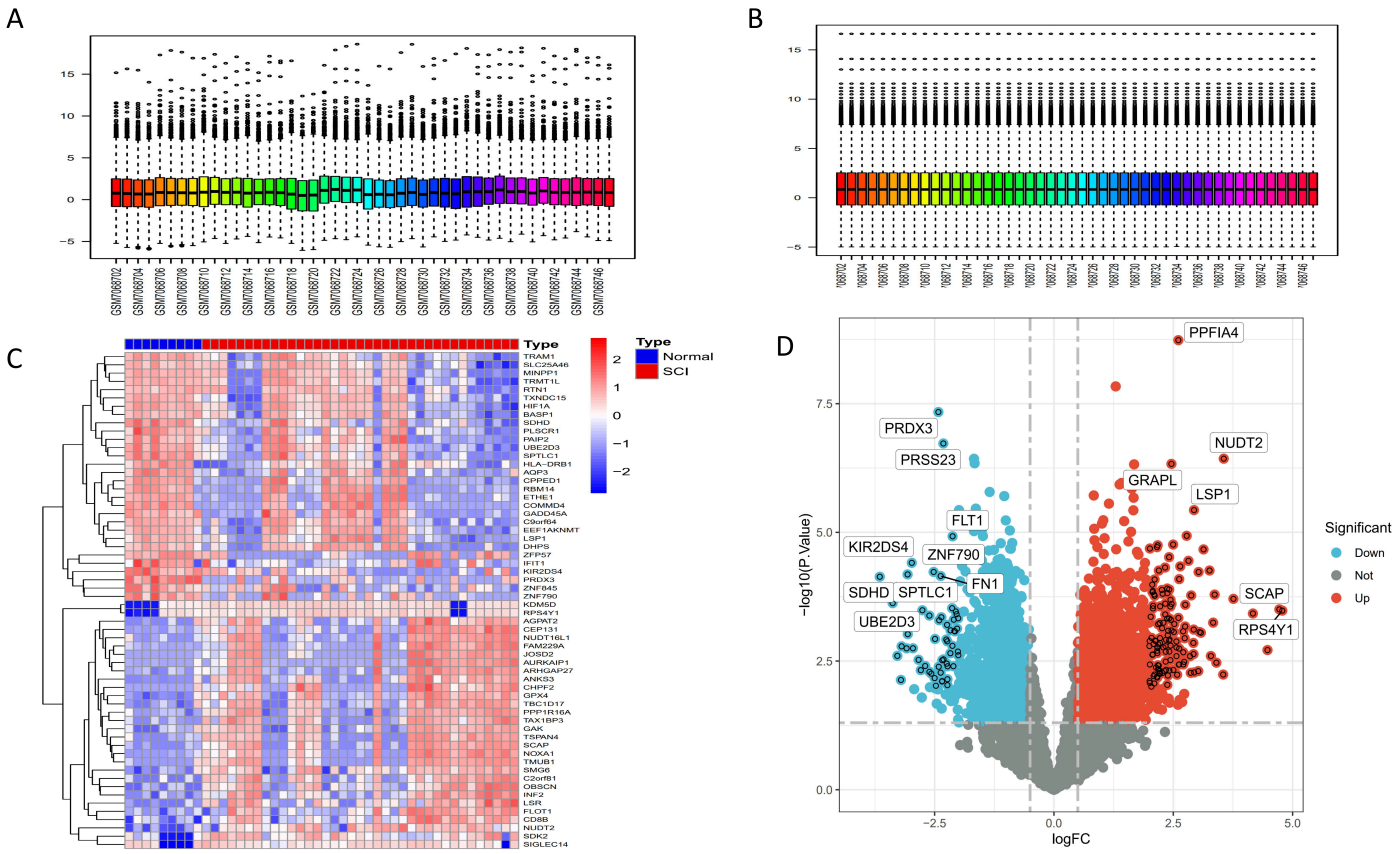


Figure 1

Screening and analysis of differentially expressed genes (DEGs) in SCI samples. (A) Data before standardization, (B) Data after standardization; (C) Expression profile heatmap of 929 differentially expressed genes, where red represents upregulated genes and blue represents downregulated genes; (D) Volcano plot showing differentially expressed genes in SCI samples and control samples (log2FC>1, P<0.05), where red represents upregulated genes and blue represents downregulated genes.

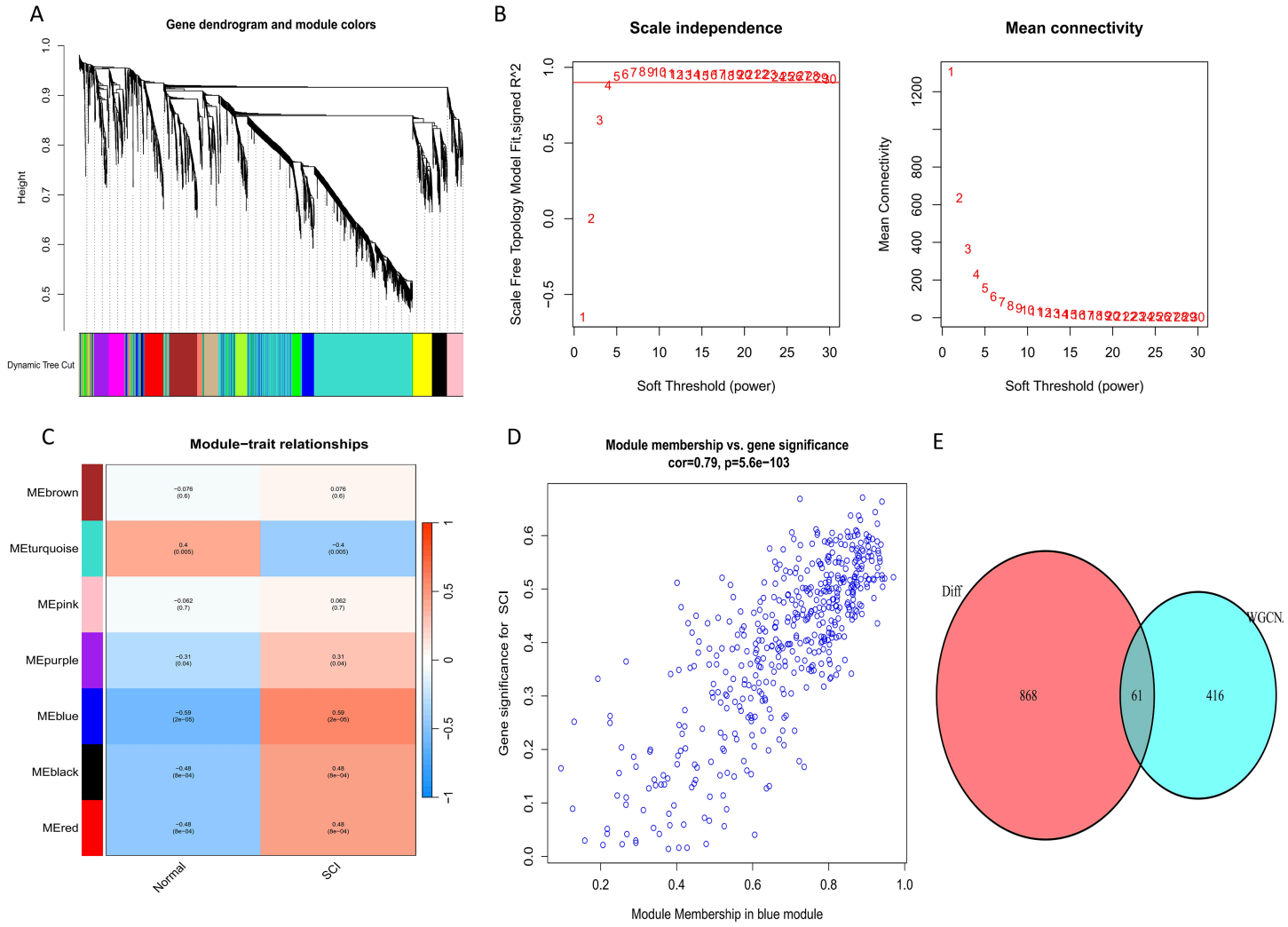


Figure 2

Weighted gene co-expression network analysis for screening core candidate genes related to SCI. (A) Gene clustering tree and module color assignment; (B) Soft threshold screening, optimal value = 5 (satisfying scale-free network characteristics); (C) Heatmap of module-SCI phenotype correlation, blue module has the strongest correlation (r=0.59, P=2e-05); (D) Correlation analysis between blue module genes and SCI (cor=0.79, P=5.6e-103); E: Intersection of blue module genes and DEGs, obtaining 61 candidate genes.

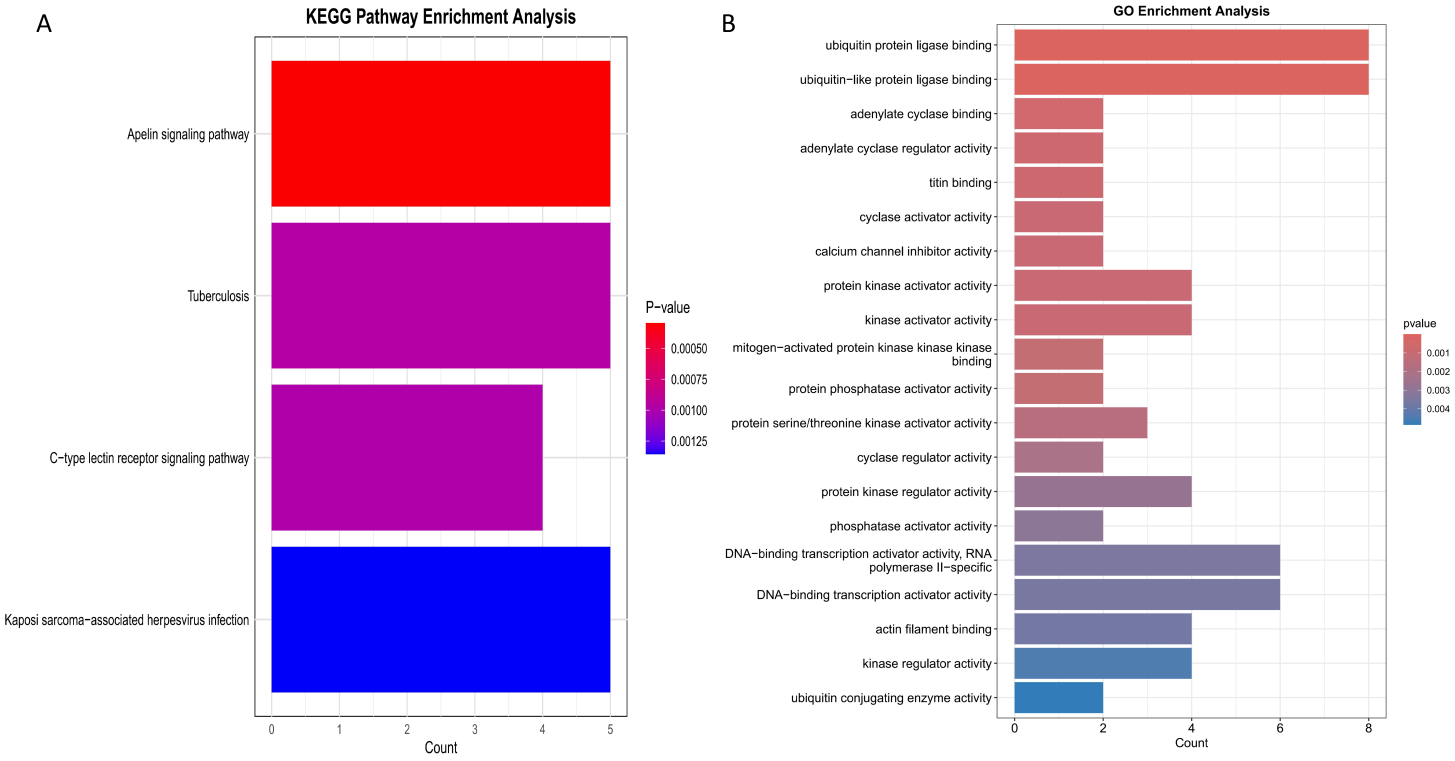


Figure 3

Functional enrichment analysis of 61 candidate genes (A) KEGG enrichment analysis (Apelin signaling pathway, C-type lectin receptor signaling pathway, etc.); (B) GO enrichment analysis (ubiquitin-protein ligase binding, adenylate cyclase regulatory factor activity, etc.).

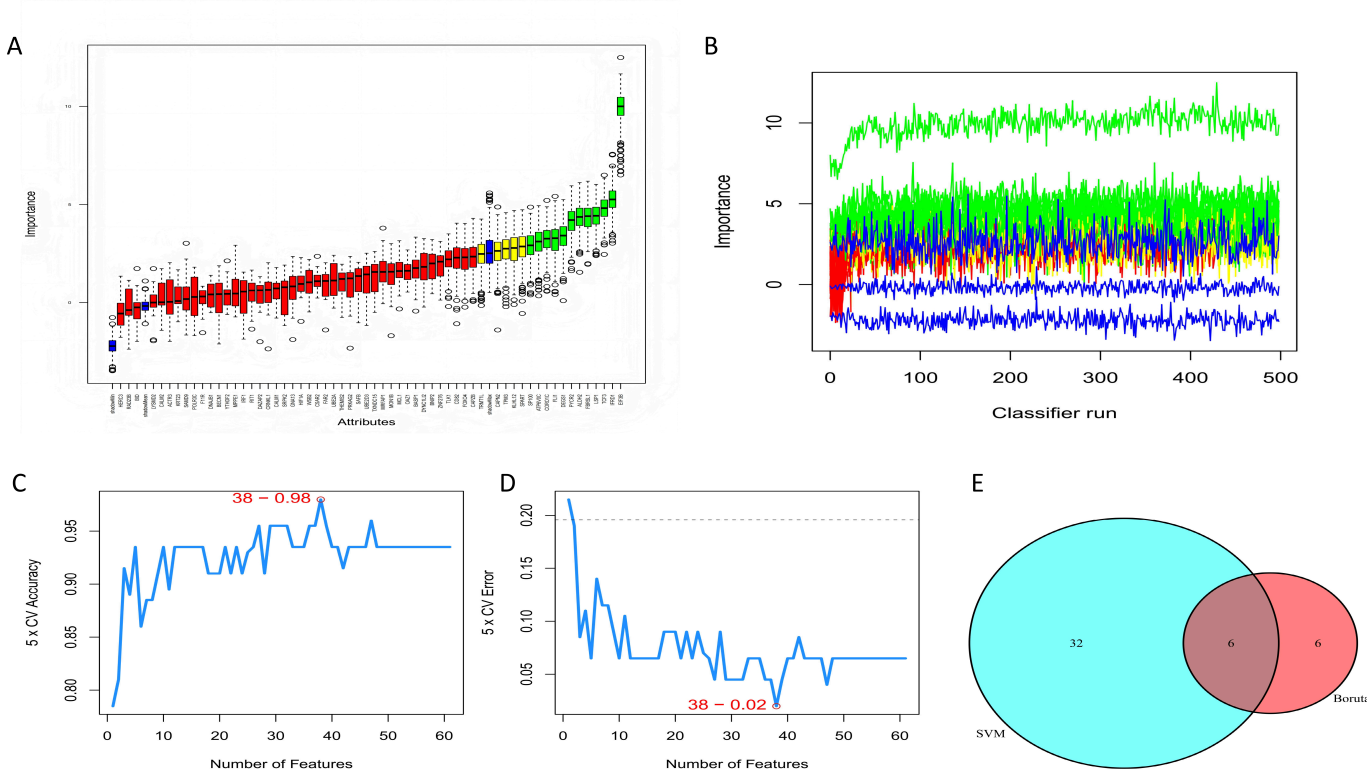


Figure 4

Candidate gene screening based on machine learning algorithms. (A) Boruta algorithm: 12 SCI-related genes were screened by sorting by Z-value; (B) Gene stability analysis based on the number of classifier runs; (C)(D) Support vector machine recursive feature elimination (SVM-RFE) algorithm: 38 feature genes were obtained, corresponding to the highest accuracy (0.98) and the lowest error rate (0.02); (E) The intersection of the two algorithms screened genes, resulting in 6 candidate genes (EIF3B, ATP6V0C, IFRD1, LSP1, PYCR2, FBRSL1).

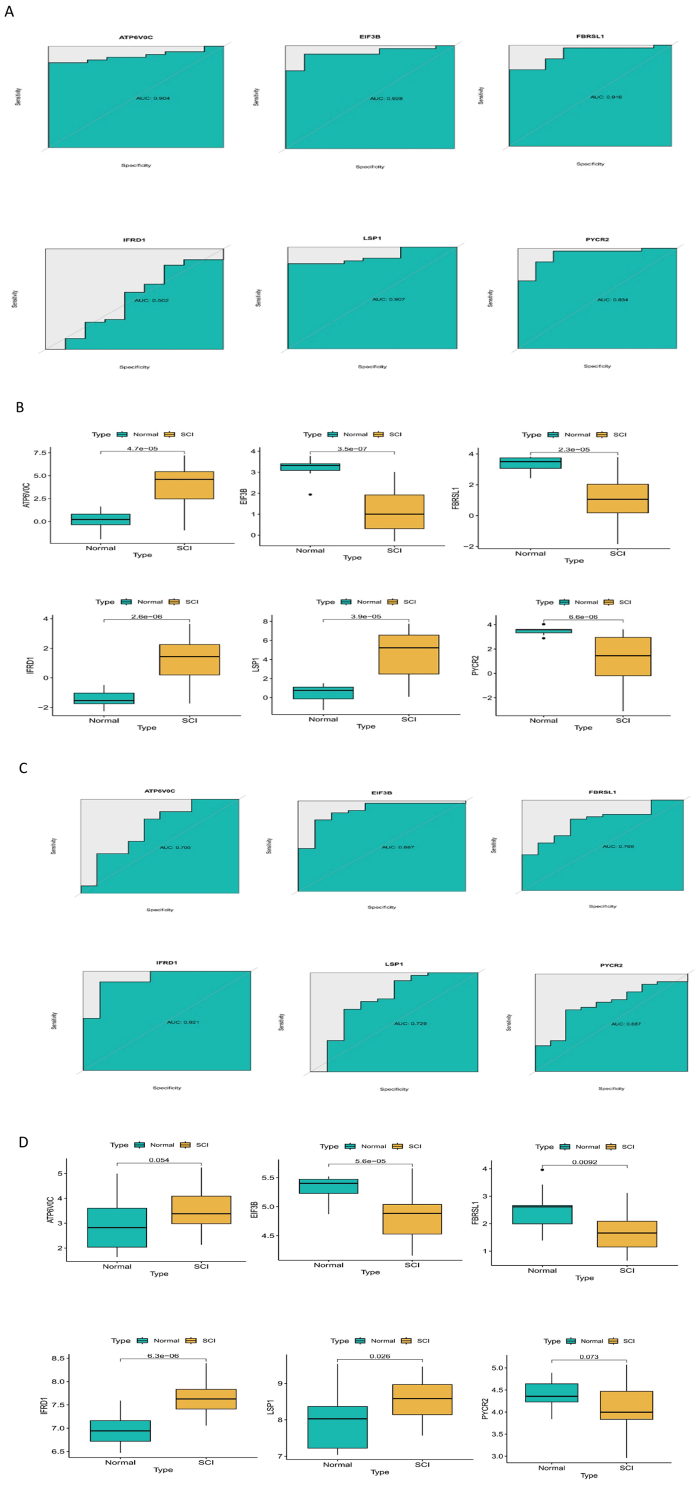


Figure 5

Expression and diagnostic value validation of 6 candidate genes. (A) Training set: expression box plot of 6 genes (downregulated expression of EIF3B, FBRSL1, and PYCR2 in the SCI group); (B) Training set: ROC curve of 6 genes (IFRD1: AUC=0.502, extremely low diagnostic value); (C) Validation set: ROC curve of 6 genes; (D) Validation set: expression box plot of 6 genes (ATP6V0C, PYCR2: P>0.05, no statistically significant difference).

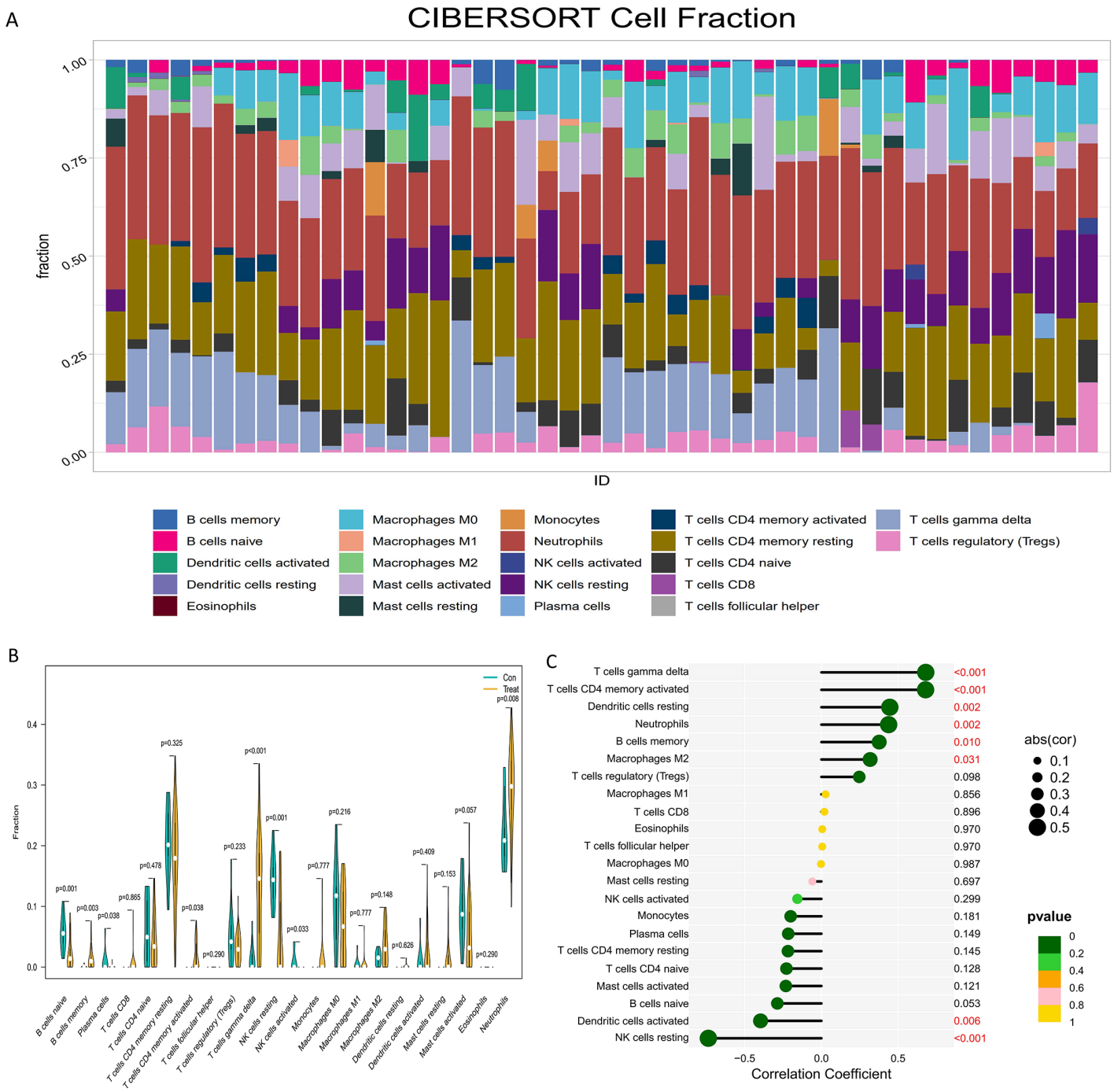


Figure 6

Correlation analysis of immune cell infiltration and LSP1 in SCI (A) Bar chart of the proportion of 22 immune cell types; (B) 13 immune cell types, including neutrophils, were significantly elevated in the SCI group; (C) LSP1 was positively correlated with neutrophils and other cells, and negatively correlated with resting NK cells and other cells.

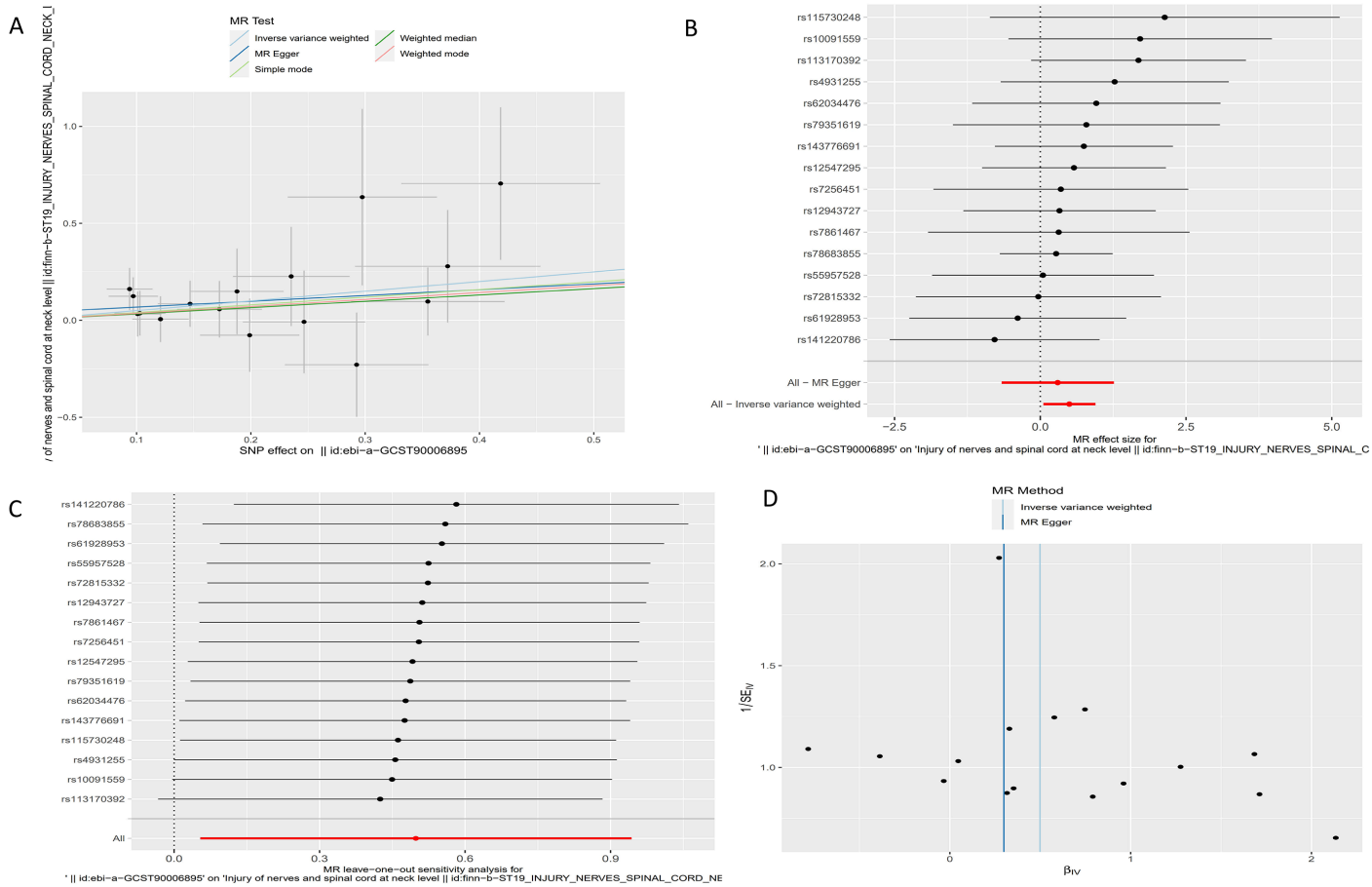


Figure 7

Mendelian randomization analysis of LSP1 and SCI (A)(B) Causal effect analysis of LSP1 on the risk of SCI (elevated LSP1 expression increases the risk of SCI); (C) Sensitivity analysis by eliminating individual SNPs one by one; (D) Heterogeneity test based on funnel plot combined with MR-Egger intercept test.

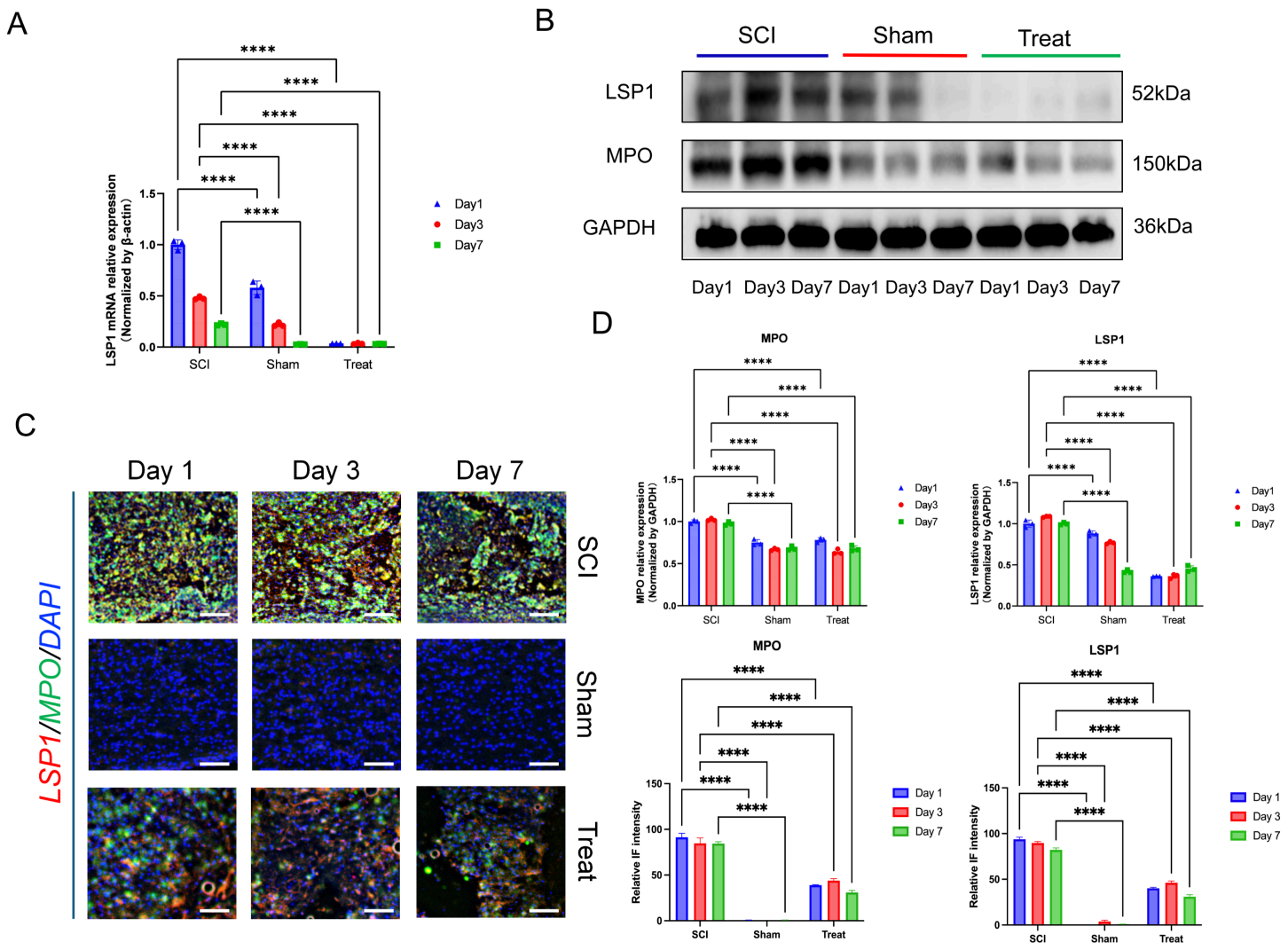


Figure 8

Dynamic expression of LSP1 after SCI in mice and its correlation with MPO expression. (A) mRNA expression level of LSP1 in LSP1$^{+/+}$ mice; (B) WB bands of LSP1 and MPO proteins; (C) Fluorescence patterns of LSP1 and MPO proteins; (D) Difference in MPO protein expression between LSP1$^{+/+}$ and LSP1$^{-/-}$ mice. ****P < 0.0001.

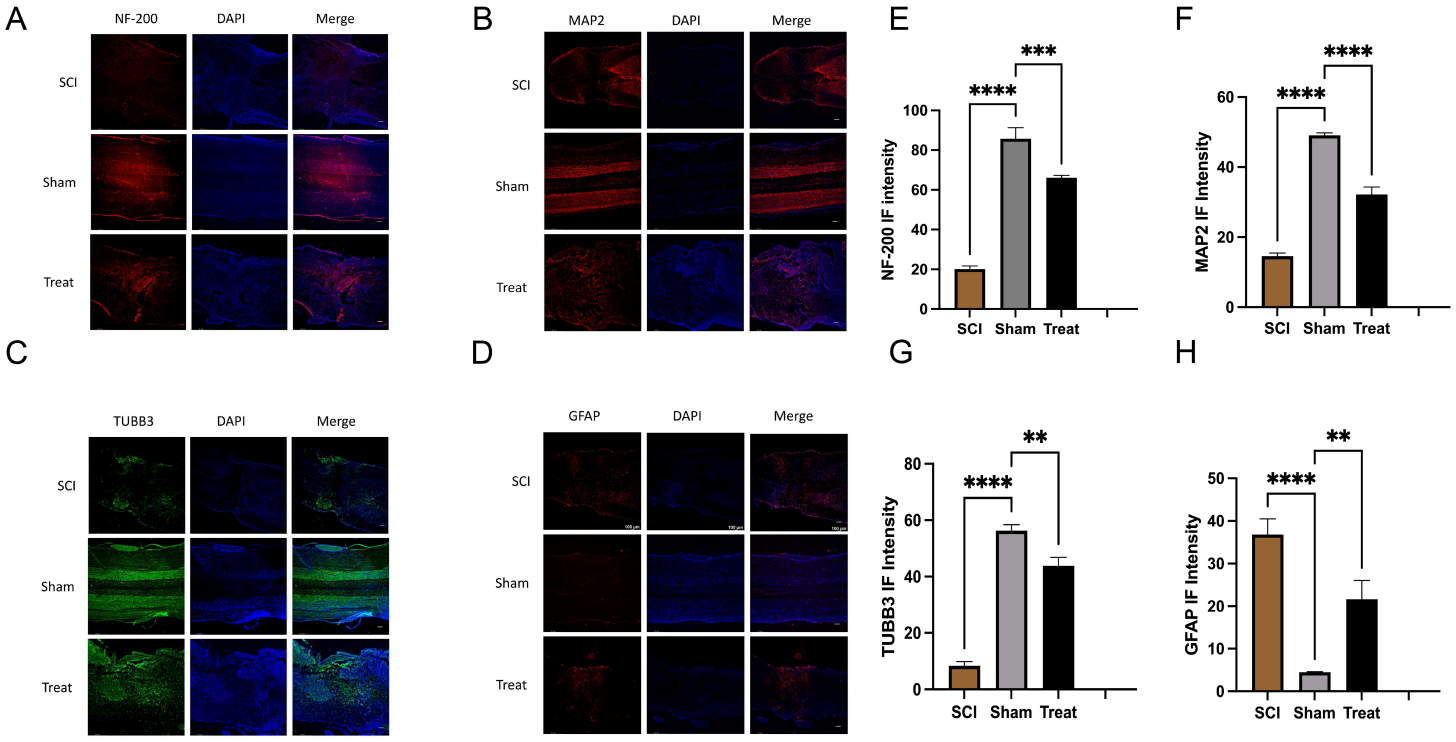


Figure 9

Effects of LSP1 knockout on neural repair and glial scar formation after SCI in mice. (A) NF-200 immunofluorescence staining (axons/neurofilaments); (B) MAP2 immunofluorescence staining (newborn neurons); (C) TUBB3 immunofluorescence staining (neurons); (D) GFAP immunofluorescence staining (glial scars). (E)(F)(G)(H) Statistical analysis of fluorescence values in each group. Scale bar: 100 μm; **P<0.01;*P<0.001;****P<0.0001.**

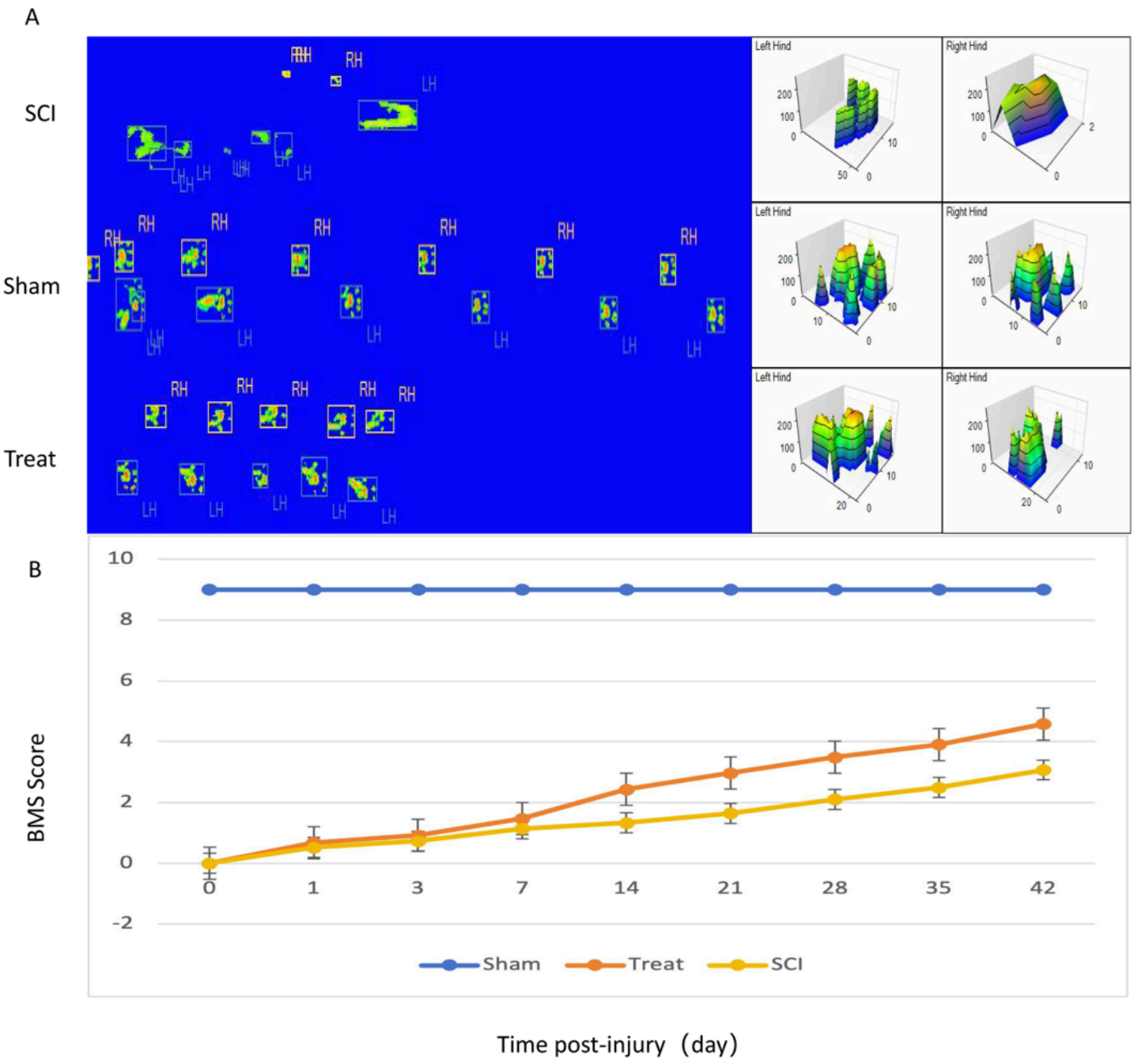


Figure 10

Effect of LSP1 knockout on motor function recovery after SCI in mice: (A) Gait performance of mice in each group, including Sham group, SCI group, and LSP1 knockout SCI group (LSP1$^{-/-}$ SCI group, labeled Treat in the figure). Typical gait disorder was observed in the SCI group; (B) Dynamic monitoring of BMS motor function scores of mice in wild-type SCI group and Treat group. The vertical axis is the BMS score (0-9 points), and the horizontal axis is the number of days after surgery (0, 1, 3, 7, 14, 21, 28, 35, 42 days). Compared with Sham group, $P<0.05$, and compared with LSP1$^{+/+}$ SCI group, $P<0.05$.

Supplementary Files

This is a list of supplementary files associated with this preprint. Click to download.

- Appendix1.BasicinformationaboutLSP1IVs.xlsx